Society of Medical Education & Research

2021, Volume 1, Page No: 119-136
ISSN: 3108-4834

Archive of International Journal of Cancer and Allied Science

Silencing JNK Potentiates CAR-T Cell–Mediated Tumor Killing by Augmenting NFATc1-Driven Transcriptional Programs in Preclinical Ovarian Cancer Models

Helena Sofia Martins[1]*, Ana Rita Teixeira[1], Daniel Mark Johnson[2], Ethan Robert Williams[2]

[1]Institute of Molecular Pathology and Immunology, University of Porto, Porto, Portugal.
[2]Department of Oncology, Johns Hopkins University School of Medicine, Baltimore, United States.

***E-mail** ✉ h.martins.ipatimup@gmail.com

Abstract

Improving the activity of chimeric antigen receptor T (CAR-T) cell therapy in solid cancers represents a critical unmet need in oncology. Because nuclear factor of activated T cells (NFAT) signaling governs multiple aspects of T cell behavior, we proposed that selective control of NFAT activity via inhibition of c-Jun N-terminal kinases (JNK) could reprogram CAR-T cells toward superior tumor-eliminating capacity. A lentiviral system encoding short-hairpin RNA was established to achieve durable JNK suppression in CAR-T cells. Human epidermal growth factor receptor 2–specific CAR-T cells were generated from peripheral blood T cells and evaluated using functional assays in vitro as well as two independent human ovarian cancer xenograft models.

CAR-T cells with reduced JNK expression exhibited diminished antigen-driven activation and lower helper T cell cytokine output but demonstrated markedly enhanced cytotoxic activity against tumor cells both in culture and in vivo. Mechanistic analyses showed that JNK silencing reoriented NFAT signaling toward preferential NFATc1-dependent transcription, resulting in increased granzyme B production. JNK functions as a central signaling checkpoint that restrains CAR-T cell cytotoxicity, and its inhibition offers a rational strategy to directly amplify CAR-T antitumor efficacy in human cancer treatment.

Keywords: Immunotherapy, Chimeric Antigen Receptor (CAR), T cell, Ovarian cancer

Introduction

A variety of approaches have been pursued to extend the success of chimeric antigen receptor T (CAR-T) cell therapy beyond hematologic malignancies and into solid tumors. Strategies such as cytokine supplementation [1], combination with immune checkpoint inhibitors [2], and transcriptional reprogramming of CAR-T cells [3, 4] have demonstrated improvements in persistence, tumor infiltration, and stem-like features. Despite these advances, achieving consistent and durable tumor control remains challenging, largely due to insufficient optimization of CAR-T cell function within the tumor microenvironment.

NFAT transcription factors comprise five isoforms—NFATc1 through NFATc4 and TonEBP [5]—that exert distinct and sometimes opposing roles in T cell biology. NFATc1 has been associated with cytotoxic effector function [6], whereas NFATc2 contributes to dysfunctional or exhausted T cell states [7]. Consequently, fine-tuning NFAT signaling represents a promising but underdeveloped strategy to enhance CAR-T cell performance. Current interventions generally aim to suppress NFAT activity to prevent excessive activation [8], yet methods capable of selectively optimizing NFAT isoform activity remain poorly defined.

c-Jun N-terminal kinases (JNK) act as upstream modulators of NFAT signaling [9, 10]. Specifically, JNK restricts NFATc1 activity by inhibiting its nuclear translocation [9, 10], while simultaneously promoting

Access this article online https://smerpub.com/

Received: 29 January 2021; **Accepted:** 18 April 2021

How to cite this article: Martins HS, Teixeira AR, Johnson DM, Williams ER. Silencing JNK Potentiates CAR-T Cell–Mediated Tumor Killing by Augmenting NFATc1-Driven Transcriptional Programs in Preclinical Ovarian Cancer Models. Arch Int J Cancer Allied Sci. 2021;1:119-36. https://doi.org/10.51847/8gPM3QLi9R

NFATc2 transcriptional activity through phosphorylation of its regulatory N-terminal domain [11]. Through these divergent effects, JNK signaling has the potential to skew T cell functional outcomes. Although JNK is essential during early T cell activation and priming [12], its role in regulating the effector functions of already activated T cells, including CAR-T cells, has not been fully characterized.

Ovarian cancer xenograft models were selected to investigate strategies for enhancing CAR-T cell efficacy in solid tumors. This malignancy is frequently diagnosed at advanced stages and exhibits high rates of therapeutic resistance [13], underscoring the need for alternative treatment approaches. Although ovarian tumors are often heavily infiltrated by immune cells, they generally fail to respond to immune checkpoint blockade, in part due to limited numbers of tumor-reactive T cells [14]. CAR-T cell therapy circumvents this limitation by providing antigen-specific T cells; however, clinical response rates in ovarian cancer remain modest at approximately 20% [15]. Therefore, while CAR-T therapy is conceptually attractive for ovarian cancer, substantial optimization is still required.

Based on these observations, we hypothesized that suppressing JNK signaling could reprogram NFAT activity in CAR-T cells and thereby enhance their antitumor function in ovarian cancer. To test this hypothesis, we systematically examined the impact of JNK knockdown on CAR-T cell activation, transcriptional signaling, and antitumor efficacy using complementary in vitro assays and in vivo ovarian cancer models.

Materials and Methods

Study design

The consequences of JNK suppression on CAR-T cell activation and antitumor performance were evaluated using human ovarian cancer xenografts and cell-based experimental systems. CAR-T cells were generated from peripheral blood T cells obtained from healthy donors.

Cell culture

HEK293T, SKOV3, OVCAR8, and Jurkat cell lines were purchased from the American Type Culture Collection and maintained in Iscove's Modified Dulbecco's Medium supplemented with fetal bovine serum, GlutaMAX, and antibiotic–antimycotic solution. Cells were cultured at 37 °C under 5% CO_2.

Lentiviral vector construction

Lentiviral particles were produced in HEK293T cells via calcium phosphate–mediated transfection [16], concentrated by ultracentrifugation, and stored at −80 °C. CAR constructs **(Figure 1d)** coexpressed short-hairpin RNAs targeting JNK or a scrambled control under the H1 promoter, ZsGreen under the EF1α promoter, and the CAR transgene under the murine stem cell virus promoter. For NFATc1 overexpression, vectors encoded NFATc1-P2A-mCherry driven by EF1α. NFAT transcriptional activity was monitored using a luciferase reporter containing nine tandem antigen receptor response elements controlling Akaluc expression under a minimal interleukin-2 promoter [17]. NFATc1 and NFATc2 gene disruption was achieved using single guide RNAs designed with GenCRISPR and delivered via the pLENTICRISPRv2 system [18].

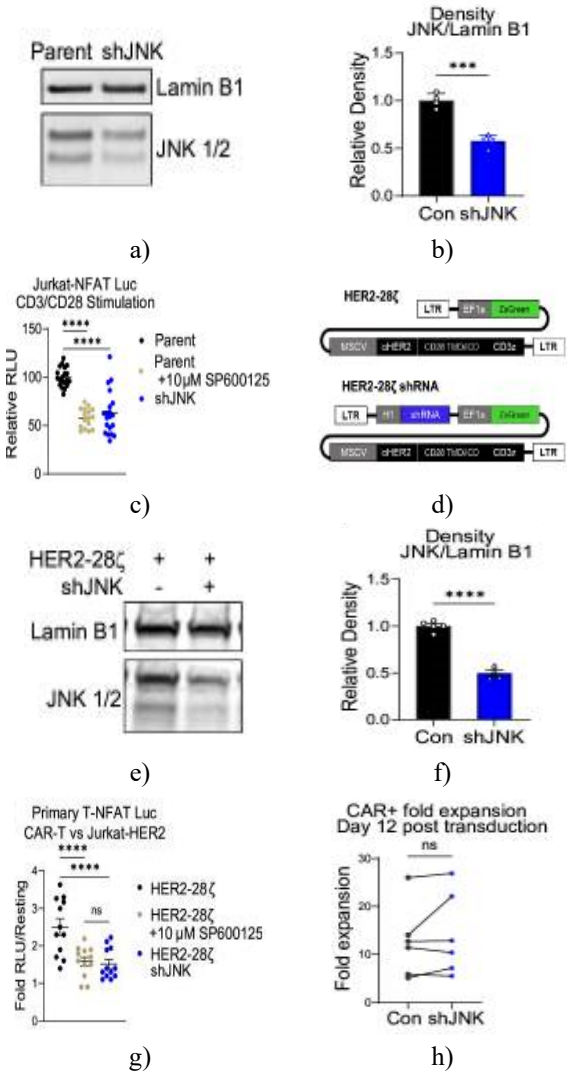

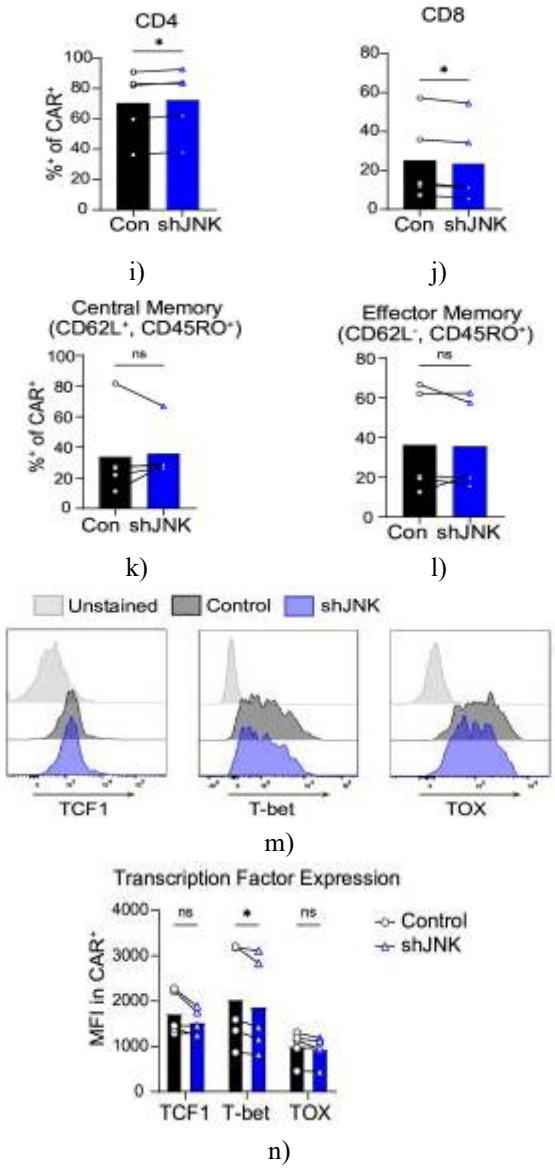

Figure 1. Attenuation of JNK signaling limits CAR-associated NFAT activity while preserving CAR-T cell generation. (a–b) A lentiviral shJNK construct was introduced into Jurkat NFAT-Luc reporter cells, after which JNK protein abundance was quantified by immunoblotting. Experiments were repeated twice, each with two technical replicates. Representative membranes (a) display total JNK1/2 alongside LaminB1 as a loading control, and corresponding densitometric analyses are summarized in (b). Statistical evaluation was conducted using an unpaired t-test with Welch's correction. (c) Cells described in (a) were stimulated using 2.5 percent (w/v) ImmunoCult CD3/CD28 antibody complexes, either alone or combined with the JNK inhibitor SP600125 (10 μM), and NFAT-driven luciferase output was subsequently measured. Five independent experiments were performed. Data are shown as pooled values, with individual points representing luminescence normalized to the mean signal from parental control wells. Group comparisons were analyzed using one-way ANOVA followed by Fisher's LSD post hoc testing. (d) Overview of lentiviral CAR expression vectors, illustrating constructs with or without an shRNA module encoding either a scrambled control sequence or shJNK. (e–f) CAR-T cells generated using either control or shJNK-containing vectors were harvested 12 days after transduction for immunoblot analysis. Samples were obtained from two independent donors, each analyzed with two to three technical replicates. Representative immunoblots (e) show total JNK1/2 and LaminB1, and aggregated densitometric quantification is presented in (f). Statistical analysis was performed using an unpaired t-test with Welch's correction. (g) Control or shJNK CAR-T cells were cotransduced with an NFAT-Luc reporter and incubated with Jurkat-HER2 target cells at a 1:1 ratio, in the presence or absence of SP600125 (10 μM). Luminescence measurements were obtained from three donors with four technical replicates per donor. Results are displayed as fold induction relative to unstimulated controls. Statistical significance was assessed by one-way ANOVA with Fisher's LSD test. (h) Proliferative expansion of control versus shJNK CAR-T cells was quantified on day 12 following transduction. Data from six donors are shown and analyzed using a paired ratio t-test. (I–N) Immunophenotypic characterization of CAR-T cells was performed by flow cytometry on day 12 post-transduction using samples from five donors. Paired ratio t-tests were applied. Scatter plots depict the fraction of ZsGreen$^+$ CAR-T cells expressing CD4 (i), CD8 (j), CD62L$^+$/CD45RO$^+$ central memory markers (k), or CD62L$^-$/CD45RO$^+$ effector memory markers (l). Representative intracellular staining histograms are shown in (m), with corresponding mean fluorescence intensity (MFI) values summarized in (n).

Abbreviations: ANOVA= analysis of variance; CAR-T= chimeric antigen receptor T; HER2= human epidermal growth factor receptor 2; ICD= intracellular domain; JNK= c-Jun N-terminal kinases;

LSD= least significant difference; LTR= long terminal repeats; MFI, mean fluorescence intensity; MSCV, murine stem cell virus; NFAT-Luc= nuclear factor of activated T cells–luciferase; RLU= relative light units; shRNA= short-hairpin RNA; TMD= transmembrane domain. *p<0.05, ***p<0.001, ****p<0.0001.

Human peripheral blood mononuclear cell isolation

Peripheral blood mononuclear cells (PBMCs) were derived from freshly collected leukocyte retention system cones obtained from LifeSouth Community Blood Centers (Gainesville, Florida, USA). Following washing with phosphate-buffered saline, erythrocytes were removed by chemical lysis using PharmLyse (BD Biosciences #555899). Isolated PBMCs were cryopreserved in Bambanker Freezing Medium (Bulldog Bio #BB01) until use.

Primary T cell culture and experimental procedures

T cells were maintained in Iscove's Modified Dulbecco's Medium supplemented with 5 percent (v/v) human AB serum, 1 percent GlutaMAX, and 1 percent antibiotic–antimycotic solution. For activation, 6×10^6 PBMCs were incubated for 36 hours with anti-mouse IgG–coated magnetic beads conjugated with αCD3 (BioLegend #300333) and αCD28 (BioLegend #302943) antibodies, followed by magnetic bead removal. Activated T cells were exposed to concentrated lentiviral preparations for 2 hours in the presence of polybrene. Cells were subsequently expanded for 12 days in culture medium containing interleukin-7 and interleukin-15. CAR expression was tracked via ZsGreen fluorescence. Unless otherwise indicated, functional assays were conducted using 1.5×10^5 T cells per well in 96-well plates supplemented with recombinant human IL-2. Stimulatory conditions included ImmunoCult αCD3/αCD28 antibody complexes, biotinylated recombinant human HER2-Fc chimera, αCD3 antibody, or αCD28 antibody, as specified in individual figure legends. SP600125 was applied as indicated. For experiments using resting T cells, $CD3^+$ T cells were enriched from thawed PBMCs using the EasySep Human T Cell Enrichment Kit.

Cytotoxicity measurements

SKOV3 and OVCAR8 ovarian cancer cell lines expressing firefly luciferase [19] were seeded at 1×10^4 cells per well and cocultured with flow-sorted CAR-positive or untransduced T cells at the specified effector-to-target ratios. After 24 hours, D-luciferin substrate was added and bioluminescence was recorded using a Varioskan Lux spectrophotometer. Tumor cell killing was calculated as:

(1 − luminescence in CAR-T wells / mean luminescence of mock T cell wells at the same E:T ratio) × 100.

For assays involving purified $CD4^+$ or $CD8^+$ CAR-T subsets, total cytotoxicity was determined by comparison with tumor-only wells.

Flow cytometry and immunofluorescence analysis

Surface and intracellular staining procedures were carried out according to manufacturer protocols using PBS supplemented with fetal bovine serum, sodium azide, and EDTA. Nuclear transcription factors were detected using the True-Nuclear Transcription Factor Buffer Set, while granzyme staining employed FIX & PERM reagents. Monensin was included during CD107α mobilization assays. Samples were fixed in paraformaldehyde prior to acquisition on BD LSRFortessa or BD FACSymphony A5 cytometers. Data were analyzed using FlowJo v10. Cell sorting was performed on a BD FACSAria instrument. Immunofluorescence imaging was conducted using an EVOS M7000 microscope, and quantitative image analysis was performed with ImageJ.

Mouse husbandry

All animal experiments were reviewed and approved by the Institutional Animal Care and Use Committee of the University of Alabama at Birmingham (UAB IACUC) and were conducted in compliance with National Institutes of Health guidelines and standards established by the Association for Assessment and Accreditation of Laboratory Animal Care International. NOD.Cg-Prkdc^scid^ Il2rg^tm1Wjl^/SzJ (NSG) mice aged 8–10 weeks were used throughout the study. Animals were maintained in sterile, autoclaved cages equipped with individual ventilated isolators. Mice were provided irradiated standard rodent chow (LabDiet 5LJ5) and Hydropac water ad libitum.

In vivo antitumor efficacy in human ovarian cancer xenograft models

For the intraperitoneal SKOV3 model, NSG mice received 1×10^6 $mCherry^+$ firefly luciferase–expressing SKOV3 cells by intraperitoneal injection. Fourteen days later, mice were treated with 1×10^6 CAR^+ T cells

administered intravenously. Tumor progression was monitored via bioluminescent imaging following intraperitoneal injection of D-luciferin using an IVIS Lumina III imaging system (PerkinElmer #CLS136334). Animals were followed until day 70 or until reaching predefined humane endpoints in accordance with UAB IACUC approval.

For the OVCAR8 xenograft model, 5×10^5 mCherry$^+$ firefly luciferase–labeled OVCAR8 cells were implanted subcutaneously in a 1:1 mixture with Matrigel (Corning #356255). Three days after tumor implantation, mice received 1.5×10^6 CAR$^+$ T cells intravenously. Tumor dimensions were measured using calipers, and tumor volume was calculated using the formula $V = (1/2) \times (\text{length} \times \text{width}^2)$. Animals were maintained until day 33 after CAR-T cell infusion. Tumor volume did not exceed the predefined maximum of 2000 mm^3 in any animal. Mice were euthanized if tumor-associated symptoms developed, including ascites or deterioration in body condition. Animals were randomized into treatment groups based on tumor size, housed in mixed cohorts to reduce confounding variables, and none were excluded following treatment initiation. Blinding was not applied during these studies.

Ex vivo quantification of CAR-T cells

Prior to tissue harvest, mice were perfused to remove circulating blood. Omental tumor tissues were enzymatically dissociated in IMDM supplemented with 5% bovine serum albumin, Liberase TH (2 ng/mL; Roche #12352200), and DNase I (10 U/mL; Thermo Scientific #EN0521). Absolute CAR-T cell numbers were determined using Precision Count Beads (BioLegend #424902).

Luminescence assay

NFAT-Luc–transduced primary T cells were plated at 1×10^5 cells per well, whereas Jurkat-NFAT-Luc cells were plated at 0.5×10^5 cells per well in round-bottom 96-well plates. Cells were stimulated overnight under experimental conditions specified in each assay. Following stimulation, cells were lysed using buffer containing 1% Triton X-100. Lysates were clarified by centrifugation and combined with luciferase assay buffer containing ATP (2 mM) and Akalumine hydrochloride substrate (100 µM; MedChemExpress #HY-112641A). Luminescence was quantified using a Varioskan Lux spectrophotometer.

Cytokine quantification by ELISA

CAR-T cells (2×10^5) were cocultured with an equal number of Jurkat-HER2 cells in 200 µL IMDM supplemented with 5% human AB serum for 48 hours in round-bottom 96-well plates. Following centrifugation at 2000 × g, culture supernatants were collected and analyzed by multiplex ELISA through EVE Technologies (Alberta, Canada; #HD15).

Western blot analysis

Protein immunoblotting was performed as previously described [20]. Signal development was achieved using Pierce ECL Plus substrate (Thermo Scientific #32134). Fluorescent signals were captured on an iBright FL1500 imaging system (Invitrogen #A44241). Band intensity was quantified by densitometric analysis using ImageJ software.

Statistical analysis

All statistical analyses were performed using Prism v10 (GraphPad, Boston, Massachusetts, USA). Data are presented as means, with error bars indicating the SEM. Statistical tests applied to individual experiments are specified in the corresponding figure legends. All tests were two-tailed, and p values <0.05 were considered statistically significant. Significance thresholds were defined as follows: not significant ($p>0.05$), *$p<0.05$, **$p<0.01$, ***$p<0.001$, ****$p<0.0001$.

Ordinary differential equation modeling of CAR-T cell therapy

Mathematical modeling was based on Lotka–Volterra–type equations [21] and adapted from previously published CAR-T–focused ODE frameworks, including CAR-T Math [22]. Simulations were executed in RStudio using the DeSolve package [23]. Model parameters were estimated or manually adjusted to fit observed tumor growth curves. Per-cell cytotoxicity rates were derived from in vitro killing assays against OVCAR8 cells at an effector-to-target ratio of 2:1 and extrapolated to a single-cell basis. Model fitting was performed using tumor growth data from the OVCAR8 xenograft model treated with shJNK CAR-T cells.

RNA sequencing and bioinformatic analysis

Flow-sorted CD8$^+$ CAR-T cells were stimulated overnight using plate-bound HER2-Fc protein prior to RNA extraction. Total RNA was isolated with the Direct-zol RNA Miniprep Plus kit (Zymogen #R2050). Libraries

were prepared following poly-A selection and sequenced on the NovaSeq X Plus platform (paired-end reads; six gigabytes per sample) by Novogene (Sacramento, California, USA). Raw sequencing data were processed using HISAT2, featureCounts, and DESeq2 pipelines. Gene set variation analysis (GSVA) was conducted using FPKM-normalized data with the GSVA R package. NFATc1-associated [16, 24] and c-Jun-associated [25] gene sets were generated from publicly available chromatin immunoprecipitation datasets. Peak calling was performed with MACS2, and gene annotation was carried out using ChIPseeker via the Galaxy platform.

Results and Discussion

JNK blockade attenuates CD3-dependent NFAT reporter activation

NFAT transcription factors are central regulators of T cell activation and effector function [7]. To quantify NFAT signaling, Jurkat T cells expressing an NFAT-responsive luciferase reporter (Jurkat-NFAT-Luc) were employed. Stimulation with ionomycin produced a greater than 22-fold increase in reporter activity compared with unstimulated or PMA-treated controls, confirming robust NFAT responsiveness.

Given the documented regulatory interplay between JNK and NFAT signaling pathways [9, 10], we examined whether JNK inhibition alters NFAT activity. Treatment with the JNK inhibitor SP600125 [26] significantly reduced NFAT-dependent reporter activity during αCD3/αCD28 costimulation in Jurkat cells, achieving a maximal suppression of 58% and an IC_{50} of 2.754 µM. In activated primary T cells derived from PBMCs, αCD3/αCD28 stimulation induced phosphorylation of JNK and its downstream target c-Jun. Pharmacologic inhibition of JNK resulted in marked reduction of c-Jun phosphorylation and suppressed NFAT reporter activity by more than 80%, with an IC_{50} of 7.845 µM. Importantly, inhibition of NFAT signaling occurred independently of TCR signal strength or αCD28 costimulation, indicating that JNK activity is primarily responsive to CD3 engagement. Collectively, these data demonstrate that JNK inhibition selectively suppresses CD3-driven NFAT transcriptional activity in primary human T cells.

JNK knockdown via shRNA attenuates CAR-driven NFAT signaling

To explore modulation of NFAT activity through JNK suppression, we noted that conventional pharmacologic inhibitors of JNK are limited by specificity and potency [27]. As an alternative, we engineered a lentiviral short-hairpin RNA (shRNA) targeting both JNK1 and JNK2 (shJNK; sequence GATCATGAAAGAATGTCCTA). In Jurkat-NFAT-Luc cells, shJNK reduced JNK protein levels by approximately 50% and diminished NFAT reporter activity by 42% under αCD3/αCD28 costimulation, closely matching the 37% reduction observed with 10 µM SP600125 **(Figures 1a–1c)**. These results confirm that JNK positively regulates TCR-driven NFAT activation, which can be effectively suppressed via targeted knockdown or pharmacologic inhibition.

Given that CAR signaling exhibits kinetics distinct from canonical TCR stimulation [28], we tested whether JNK knockdown similarly affects CAR-induced NFAT activity. We constructed a HER2-specific CAR derived from the single-chain form of trastuzumab [29], containing a CD28 spacer, transmembrane, and intracellular domain fused to CD3ζ. This CAR (HER2-28ζ) was expressed lentivirally along with ZsGreen as a transduction marker ("CAR-T cells"), or coexpressed with shJNK ("shJNK CAR-T cells") **(Figure 1d)**. In primary human CAR-T cells, shJNK decreased JNK protein by ~50% **(Figures 1e and 1f)** and reduced CAR-driven NFAT reporter activity by ~40% upon coculture with Jurkat-HER2 cells, which lack HLA class I expression [30] to prevent TCR-mediated activation **(Figure 1g)**. These findings indicate that JNK suppression, whether by knockdown or inhibition, can dampen CAR-mediated NFAT signaling in primary T cells.

JNK knockdown does not impair CAR-T cell manufacturing

We next evaluated whether shJNK expression affected CAR-T cell expansion and phenotype. JNK knockdown did not alter proliferative capacity or the CD4/CD8 ratio (control: 2.30 vs shJNK: 2.57) **(Figures 1h–1j)**. Final CAR-T products exhibited comparable differentiation, predominantly comprising central memory (CAR-T_CM: $CD62L^+/CD45RO^+$, control: 34 percent, shJNK: 36 percent) and effector memory cells (CAR-T_EM: $CD62L^-/CD45RO^+$, control: 36 percent, shJNK: 35 percent) **(Figures 1k and 1l)**. Key transcription factors regulating T cell differentiation and function—TCF1, T-bet, and TOX [31]—were expressed at similar levels across both groups **(Figures 1m and 1n)**. Control

experiments using a scrambled shRNA (shScramble) yielded analogous results. Collectively, these data demonstrate that JNK knockdown does not compromise CAR-T production or differentiation profiles.

JNK knockdown enhances CAR-T cytotoxicity

Given NFAT's role in supporting T cell effector functions, including antigen-specific cytotoxicity [6], we assessed the functional impact of JNK knockdown on CAR-T cell killing. HER2-dependent cytotoxicity was measured against OVCAR8 and SKOV3 ovarian cancer lines, which differ in HER2 expression by nearly 40-fold (MFI 274 vs 8103) **(Figures 2a and 2b)**. Strikingly, shJNK CAR-T cells exhibited approximately a twofold enhancement in killing across both targets **(Figures 2c and 2d)**. Comparable results were observed using shScramble as a control. These observations highlight a principal advantage of JNK knockdown in CAR-T cells: a direct, robust increase in cytotoxic potency.

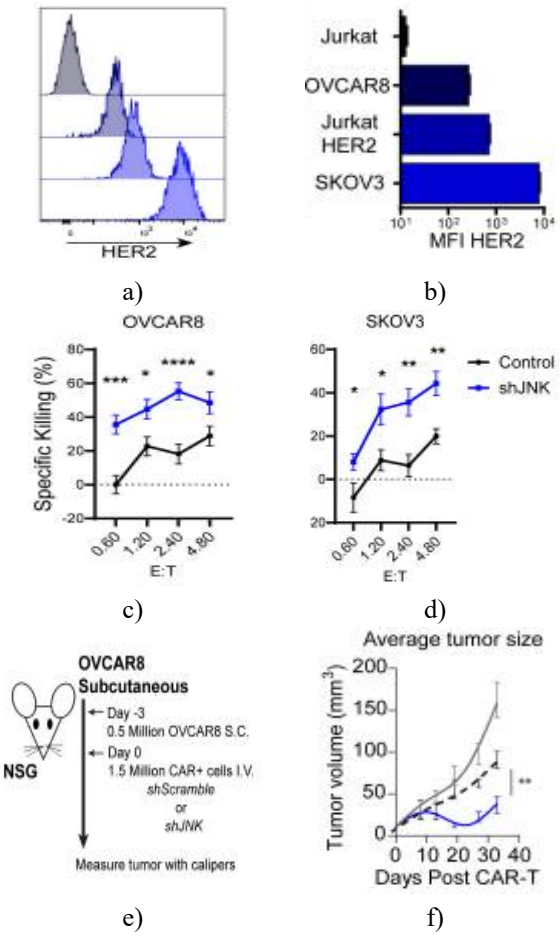

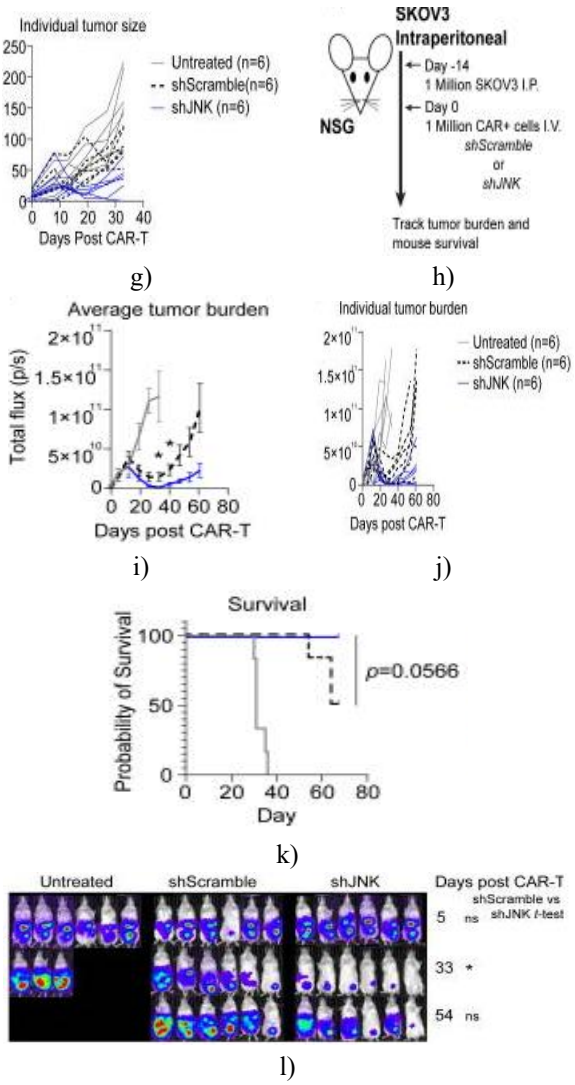

Figure 2. JNK knockdown improves CAR-T cell cytotoxicity and antitumor activity in vivo. (a–b) HER2 expression on the indicated cell lines was measured using flow cytometry, with representative histograms shown in (a) and MFI quantification in (b). (c–d) The cytotoxic potential of shJNK versus Control CAR-T cells against OVCAR8 and SKOV3 was assessed using n=3 donors, each with four technical replicates; aggregated data are shown. (e–f) Study design (e): NSG mice received 5×10^5 OVCAR8 cells subcutaneously, followed by intravenous injection of 1.5×10^6 CAR+ T cells on day 3; tumor growth was monitored via calipers. Six mice per group; results from one representative experiment of n=2 donors are presented. Average (f) and individual (g) tumor volumes are shown. (h–l) Study design (h): NSG mice were injected intraperitoneally with 1×10^6 Firefly Luciferase+

SKOV3 cells, followed by intravenous infusion of 1×10^6 CAR+ T cells on day 14. Tumor progression was quantified by bioluminescent imaging (BLI), using total photon flux (p/s) as a measure. Six mice per group; one representative experiment from n=2 donors is presented. Average (i) and individual (j) tumor burden, mouse survival (k), and representative BLI images (l) are shown. Statistical analyses: multiple unpaired t-tests with Welch's correction for tumor measurements; Log-rank test for survival. Abbreviations: BLI, bioluminescent imaging; CAR-T, chimeric antigen receptor T; E:T, effector:target; HER2, human epidermal growth factor receptor 2; I.P., intraperitoneal; I.V., intravenous; JNK, c-Jun N-terminal kinase; MFI, mean fluorescent intensity; ns, not significant; p/s, photons/s; S.C., subcutaneous; shScramble, scrambled short-hairpin RNA. *p<0.05, **p<0.01, ***p<0.001, ****p<0.0001.

JNK knockdown enhances CAR-T antitumor activity against ovarian cancer in vivo

Considering that JNK knockdown increased CAR-T cytotoxicity in vitro **(Figures 2c and 2d)** without affecting CAR-T generation **(Figures 1h–1n)**, we investigated its impact on tumor control in vivo. CAR-T cells with either shJNK or shScramble were tested against OVCAR8 tumors, a high-grade serous ovarian cancer model with moderate HER2 and low HLA-I expression [32]. From day 19, shJNK-treated mice displayed markedly reduced tumor growth, achieving a 77.5% reduction in tumor volume by day 33 compared to 44.3% in shScramble-treated mice **(Figures 2f and 2g)**. In an intraperitoneal SKOV3 model with luciferase labeling to mimic metastasis **(Figure 2h)**, shJNK CAR-T cells led to an 11.9-fold decrease in tumor burden at day 33 relative to shScramble CAR-T cells **(Figures 2i–2l)**. At the endpoint (day 70), a trend toward improved survival was noted in the shJNK group, though all mice retained some tumor. Both CAR-T types displayed similar kinetics: tumor control began around day 21, peaked by day 33, then relapsed despite continued HER2 expression and CAR-T infiltration , indicative of T cell exhaustion. Analysis of tumor-infiltrating CAR-T cells at day 21 showed CD8+ cells with T-bet+/TOX+ and T-bet−/TOX+ profiles, reflecting both retained functionality and terminal exhaustion [33, 34]. JNK knockdown did not alter the proportion of these populations, overall transcription factor levels, or exhaustion marker expression. Additionally, stemness markers CD62L and CCR7 were unchanged between groups across three sites. Together, these findings indicate that JNK knockdown strengthens CAR-T antitumor activity during early tumor engagement without modifying T cell stemness or accelerating exhaustion.

Tumor-infiltrating shJNK CAR-T cells exhibit elevated granzyme B

To determine whether enhanced cytotoxicity persists in the tumor microenvironment, CAR-T cells were analyzed 28 days post-infusion in SKOV3-bearing mice. shJNK and shScramble CAR-T cells showed comparable biodistribution across bone marrow, spleen, and omentum, suggesting that JNK knockdown does not affect CAR-T expansion or trafficking in vivo **(Figure 3a)**. Within tumors, CD8+-shJNK CAR-T cells expressed roughly twice as much granzyme B (shJNK: 24.5%+, control: 11.6%+; **(Figure 3b)**). A second donor experiment confirmed similar biodistribution **(Figure 3c)** and a persistent trend for higher tumor-specific granzyme B in shJNK CAR-T cells (average 48.2%+ versus 22.5%+ for shScramble; **(Figure 3d)**), although significance was not reached. Expression of other cytotoxic mediators, including granzyme A and Fas ligand, remained unchanged **(Figures 3e and 3f)**. These data demonstrate that JNK knockdown selectively enhances tumor-localized granzyme B production in CD8+ CAR-T cells without affecting their systemic distribution.

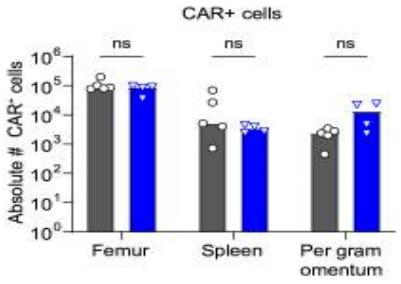

a)

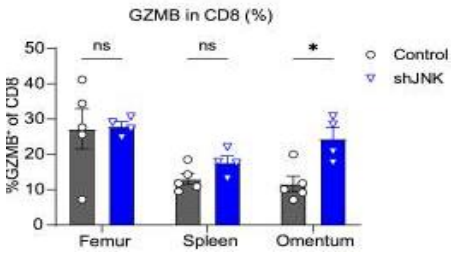

b)

Donor 1

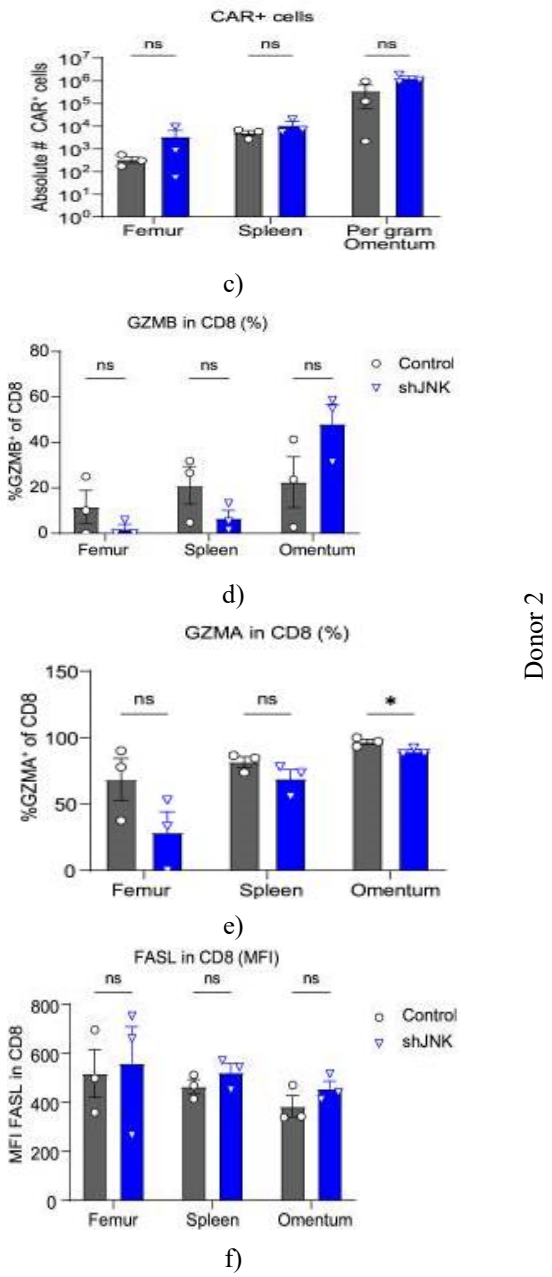

Figure 3. Tumor-infiltrating shJNK CAR-T cells exhibit increased granzyme B expression. (a–b) NSG mice were intraperitoneally engrafted with 5×10^6 Firefly Luciferase+ SKOV3 cells and received 1×10^6 CAR-T cells intravenously on day 14. Tissues were collected 28 days post-infusion. Each data point represents an individual mouse (n=5 for control CAR-T, n=4 for shJNK CAR-T). The total CAR+ cell counts per tissue (a) and the proportion of CD4− CAR-T cells expressing granzyme B (GZMB) (b) are displayed. (c–f) A second donor experiment was performed similarly (n=3 per group). Total CAR+ cell numbers per tissue (c), percentage of CD8+ CAR-T cells expressing GZMB (d), percentage of CD8+ CAR-T cells expressing granzyme A (GZMA) (e), and the mean fluorescence intensity (MFI) of Fas ligand (FASL) on CD8+ CAR-T cells (f) are shown. Statistical comparisons were performed using multiple unpaired t-tests with Welch's correction. Abbreviations: CAR-T= chimeric antigen receptor T; FASL= Fas ligand; GZMA= granzyme A; GZMB= granzyme B; IP= intraperitoneal; I.V.= intravenous; JNK= c-Jun N-terminal kinase; MFI= mean fluorescent intensity; ns= not significant; shScramble= scrambled short-hairpin RNA. *p<0.05.

JNK knockdown enhances CD8+ CAR-T cytotoxicity and degranulation activity

To determine whether increased GZMB expression results directly from JNK knockdown rather than secondary in vivo effects, CAR-T cells were stimulated in vitro with HER2-Fc protein. JNK knockdown selectively increased GZMB levels, particularly in CD8+ CAR-T cells (~1.6-fold), whereas GZMA showed a modest increase (~1.4-fold) and FASL remained unchanged **(Figures 4a–4c)**, supporting a direct link between JNK suppression and elevated cytotoxic factor expression. Enhanced GZMB levels were confirmed following co-culture with OVCAR8 or SKOV3 cells, with CD8+-shJNK CAR-T cells exhibiting more than a 1.9-fold increase in GZMB intensity in response to OVCAR8 **(Figures 4d–4f)**. Because granzyme-mediated killing depends on T cell degranulation [35], we measured CAR-T degranulation in response to HER2-Fc. JNK knockdown augmented degranulation in both CD4+ and CD8+ CAR-T populations **(Figures 4g–4i)**. Functional cytotoxicity assays using sorted populations revealed that only CD8+ CAR-T cells demonstrated significantly enhanced killing after JNK knockdown, while CD4+ CAR-T cells did not **(Figures 4j and 4k)**. Collectively, these results indicate that JNK knockdown directly promotes the cytotoxic potential of CD8+ CAR-T cells by increasing granzyme expression and degranulation activity.

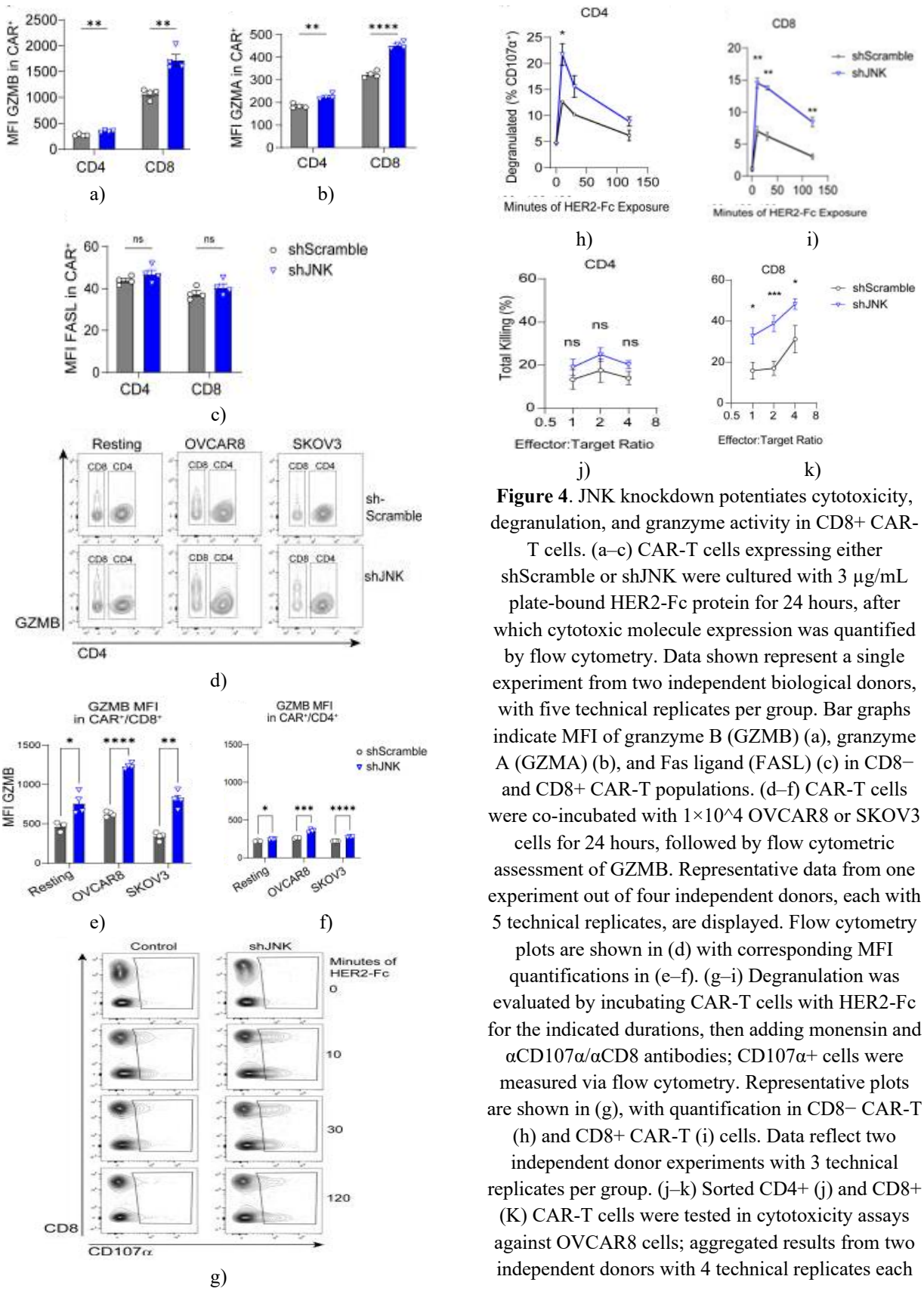

Figure 4. JNK knockdown potentiates cytotoxicity, degranulation, and granzyme activity in CD8+ CAR-T cells. (a–c) CAR-T cells expressing either shScramble or shJNK were cultured with 3 µg/mL plate-bound HER2-Fc protein for 24 hours, after which cytotoxic molecule expression was quantified by flow cytometry. Data shown represent a single experiment from two independent biological donors, with five technical replicates per group. Bar graphs indicate MFI of granzyme B (GZMB) (a), granzyme A (GZMA) (b), and Fas ligand (FASL) (c) in CD8− and CD8+ CAR-T populations. (d–f) CAR-T cells were co-incubated with 1×10^4 OVCAR8 or SKOV3 cells for 24 hours, followed by flow cytometric assessment of GZMB. Representative data from one experiment out of four independent donors, each with 5 technical replicates, are displayed. Flow cytometry plots are shown in (d) with corresponding MFI quantifications in (e–f). (g–i) Degranulation was evaluated by incubating CAR-T cells with HER2-Fc for the indicated durations, then adding monensin and αCD107α/αCD8 antibodies; CD107α+ cells were measured via flow cytometry. Representative plots are shown in (g), with quantification in CD8− CAR-T (h) and CD8+ CAR-T (i) cells. Data reflect two independent donor experiments with 3 technical replicates per group. (j–k) Sorted CD4+ (j) and CD8+ (K) CAR-T cells were tested in cytotoxicity assays against OVCAR8 cells; aggregated results from two independent donors with 4 technical replicates each

are presented. Statistical analysis used multiple unpaired t-tests with Welch's correction. Abbreviations: CAR= chimeric antigen receptor; FASL= Fas ligand; GZMA, granzyme A; GZMB= granzyme B; HER2, human epidermal growth factor receptor 2; JNK= c-Jun N-terminal kinases; MFI= mean fluorescence intensity; ns= not significant; shScramble= scrambled short-hairpin RNA. *p<0.05, **p<0.01, ***p<0.001, ****p<0.0001.

JNK knockdown preferentially amplifies cytotoxic function in CD8+ CAR-T cells

Considering that CD8+ effector T cells are inherently more cytotoxic [36], we examined whether JNK suppression preferentially enhances their activity. Upon αCD3/αCD28 costimulation, CD8+ CAR-T cells with JNK knockdown displayed approximately threefold higher GZMB levels than controls (MFI 1750 vs 658). This increase occurred across all CAR-T differentiation states—including naïve, central memory (CAR-TCM), effector memory (CAR-TEM), and effector populations—indicating that the effect of JNK knockdown on GZMB is independent of differentiation status.

NFATc1 is essential for GZMB induction following JNK knockdown

To uncover the molecular link between JNK suppression and enhanced cytotoxicity, we investigated the role of NFAT transcription factors, both known to bind the GZMB locus [6]. CRISPR-mediated knockout in Jurkat cells revealed that loss of NFATc1 abolished the upregulation of GZMB associated with JNK knockdown, whereas NFATc2 deletion paradoxically increased GZMB levels **(Figures 5a and 5b)**. These findings indicate that NFATc1 is required for the JNK knockdown-mediated increase in GZMB expression, while NFATc2 is dispensable or potentially inhibitory.

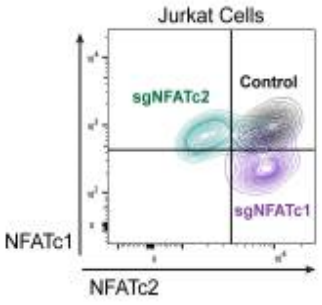

a)

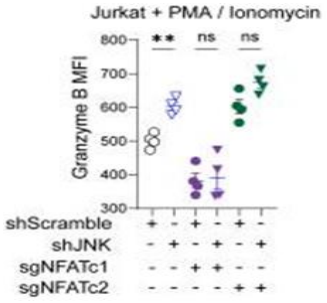

b)

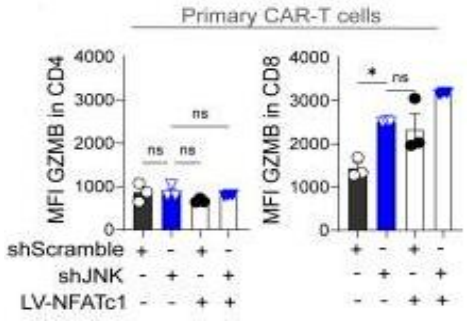

c)

Figure 5. NFATc1 mediates GZMB upregulation after JNK knockdown. (a–b) To determine the contribution of NFAT transcription factors, Jurkat T cells were genetically edited using CRISPR to delete either NFATc1 or NFATc2. Cells were then stimulated with PMA plus ionomycin in the presence of monensin for 3 hours, and intracellular granzyme B (GZMB) levels were measured by flow cytometry. Representative flow plots illustrating selective NFAT knockout are shown in (a), while GZMB quantification after stimulation is presented in (b). The dataset represents one experiment out of three independent replicates, each with four technical repeats. Brown-Forsyth and Welch ANOVA were used for statistical comparisons. (c) Primary human CAR-T cells were transduced with lentiviral constructs to overexpress NFATc1. After stimulation with 2.5% w/v Immunocult CD3/CD28 antibodies, GZMB expression was evaluated. Shown are representative flow plots from one of two independent experiments with a single donor, including three technical replicates. Abbreviations: ANOVA, analysis of variance; GZMB, granzyme B; JNK, c-Jun N-terminal kinase; MFI, mean fluorescence intensity; NFAT, nuclear factor of activated T cells; ns, not significant; shScramble, scrambled short-hairpin RNA.

NFATc1 overexpression mimics the effects of JNK knockdown on GZMB

To assess whether NFATc1 is sufficient to drive GZMB expression, we introduced NFATc1 into primary CAR-T cells. Overexpression led to increased GZMB levels in CD8+ CAR-T cells comparable to those observed after JNK knockdown **(Figure 5c)**, confirming that NFATc1 is the key mediator of GZMB induction following JNK suppression.

JNK knockdown amplifies NFATc1-dependent transcriptional activity

Building on the NFATc1-dependent GZMB upregulation, we investigated whether JNK knockdown broadly enhances NFATc1 transcriptional programs. CD8+ CAR-T cells expressing shScramble or shJNK were stimulated with HER2-Fc and subjected to bulk mRNA sequencing to characterize the transcriptional impact of JNK suppression **(Figure 6a)**.

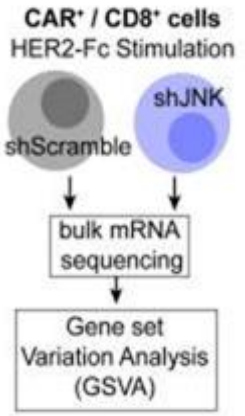

a)

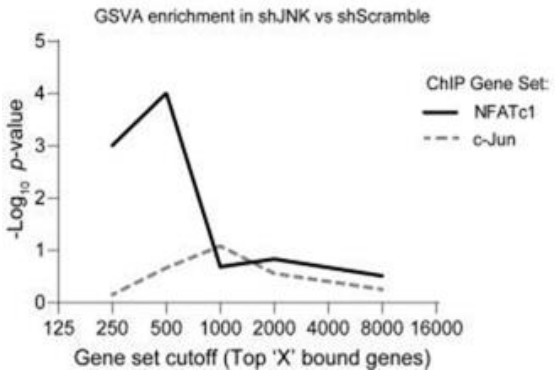

b)

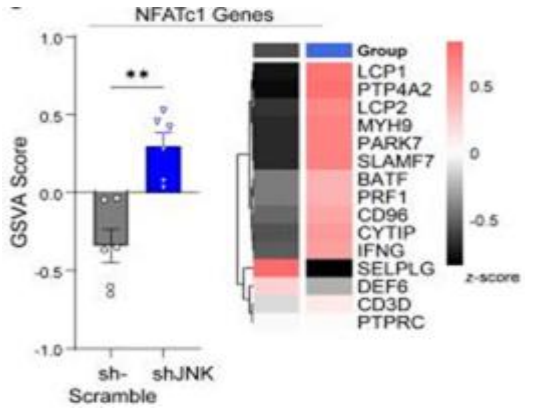

c)

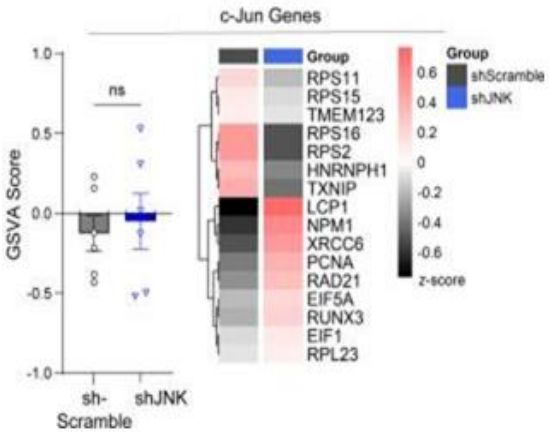

d)

Figure 6. JNK knockdown enhances NFATc1-dependent transcription. (a–d) CD8+ CAR-T cells expressing either shScramble or shJNK were stimulated for 16 hours with plate-bound HER2-Fc protein and then subjected to bulk mRNA sequencing. Gene sets for GSVA were generated using published ChIP datasets. The experiment was performed once with three independent biological donors, each with two technical replicates. Experimental schematic (s). XY plot illustrating p values from GSVA comparisons between shScramble and shJNK CAR-T cells based on ChIP datasets and MACS2 score cutoffs (b). Bar graphs and corresponding heatmaps show GSVA results for the "top 250" genes with FPKM >75 for NFATc1 (c) and c-Jun (d). Statistical analysis was performed using unpaired t-tests with Welch's correction. CAR= chimeric antigen receptor; ChIP= chromatin immunoprecipitation; FPKM= fragments per kilobase of transcript per million mapped reads; HER2= human epidermal growth factor receptor 2; JNK= c-Jun N-terminal kinases; MACS2= model-based analysis of ChIP-Seq 2; mRNA= messenger RNA;

NFAT= nuclear factor of activated T cells; ns= not significant; shScramble= scrambled short-hairpin RNA. **p<0.01.

We first conducted a broad transcriptional survey, which revealed reproducible differences across the three donors, including an approximate twofold decrease in MAPK8 (JNK1) and MAPK9 (JNK2) expression. Key transcription factors such as TBX21, EOMES, and FOXO1 were largely unaffected, whereas several cytotoxic effector genes, including GZMB and GZMA, showed upregulation following JNK knockdown. GSVA analysis confirmed that genes related to T cell migration (Gene Ontology:2000404) remained unchanged. Together, these data align with functional evidence that JNK knockdown boosts CAR-T cell cytotoxicity without altering differentiation status.

To examine NFATc1-specific transcriptional changes, we analyzed ChIP datasets for NFATc1 [24] and c-Jun [25] binding in CD8+ T cells. GSVA was performed using genes with high ChIP binding and FPKM >75 in our RNA-seq data. While c-Jun target genes were not significantly enriched, NFATc1-bound genes were strongly enriched in shJNK CAR-T cells **(Figure 6b)**. Considering the top 250 bound genes, NFATc1 targets showed significant enrichment (absolute enrichment: 0.640, p=0.001, **(Figure 6c)**), whereas c-Jun targets did not differ (absolute enrichment: 0.087, p=0.713, **(Figure 6d)**). These results suggest that JNK depletion broadly enhances NFATc1-driven transcription.

Previous reports indicate that JNK impairs NFATc1 nuclear localization by preventing its interaction with calcineurin [9, 10]. We therefore hypothesized that JNK knockdown promotes NFATc1 nuclear translocation in CAR-T cells. Immunofluorescence staining confirmed that shJNK CAR-T cells contained a higher proportion of nuclear NFATc1 compared with shScramble controls, supporting the conclusion that JNK inhibition enhances NFATc1-dependent transcription, likely via increased nuclear localization.

JNK suppression alters multiple outcomes of T cell stimulation

Despite increased GZMB expression due to NFATc1 activation, NFAT reporter activity paradoxically decreased **(Figure 1g)**. To assess overall T cell activation, we measured surface markers CD25 and CD69, which are regulated by NFAT [37]. In PBMC-derived T cells, JNK inhibition reduced CD25 and CD69 expression by roughly 45%, with similar effects across differentiation stages and both CD4+ and CD8+ T cells (. shJNK CAR-T cells stimulated with Jurkat-HER2 cells showed similar reductions in CD25 expression. Multiplex ELISA revealed that JNK knockdown lowered IL-10, IL-4, IL-5, and IL-2 by ~50%, with a trend toward decreased TNF-α, while IL-6 and IFN-γ—key mediators of cytotoxic antitumor activity [38]—were unaffected; donor-specific effects were seen for GM-CSF, IL-13, and IL-8. Overall, while cytotoxicity increased, multiple aspects of the antigen-stimulation response were suppressed, consistent with reduced NFAT reporter activity.

Mathematical modeling suggests that the direct enhancement of cytotoxicity explains enhanced tumor control

We posited that increased cytotoxicity alone could account for the superior antitumor effects of shJNK CAR-T cells. To test this, we constructed an ODE-based CAR-T model using a Lotka-Volterra predator-prey framework [21] **(Figure 7a)**. The model incorporated blood- versus tumor-localized CAR-T populations, CAR-T persistence in circulation, tumor infiltration rates, and a decay in cytotoxic function resembling exhaustion **(Figure 7b)**. Parameters were estimated, with tumor cell numbers inferred from observed tumor sizes, CAR-T cytotoxicity derived from in vitro assays, and remaining parameters fit to tumor growth curves in untreated versus shJNK-treated mice **(Figures 2e–2g)**. The model successfully recapitulated a dose-dependent response to CAR-T infusion **(Figure 7c)**.

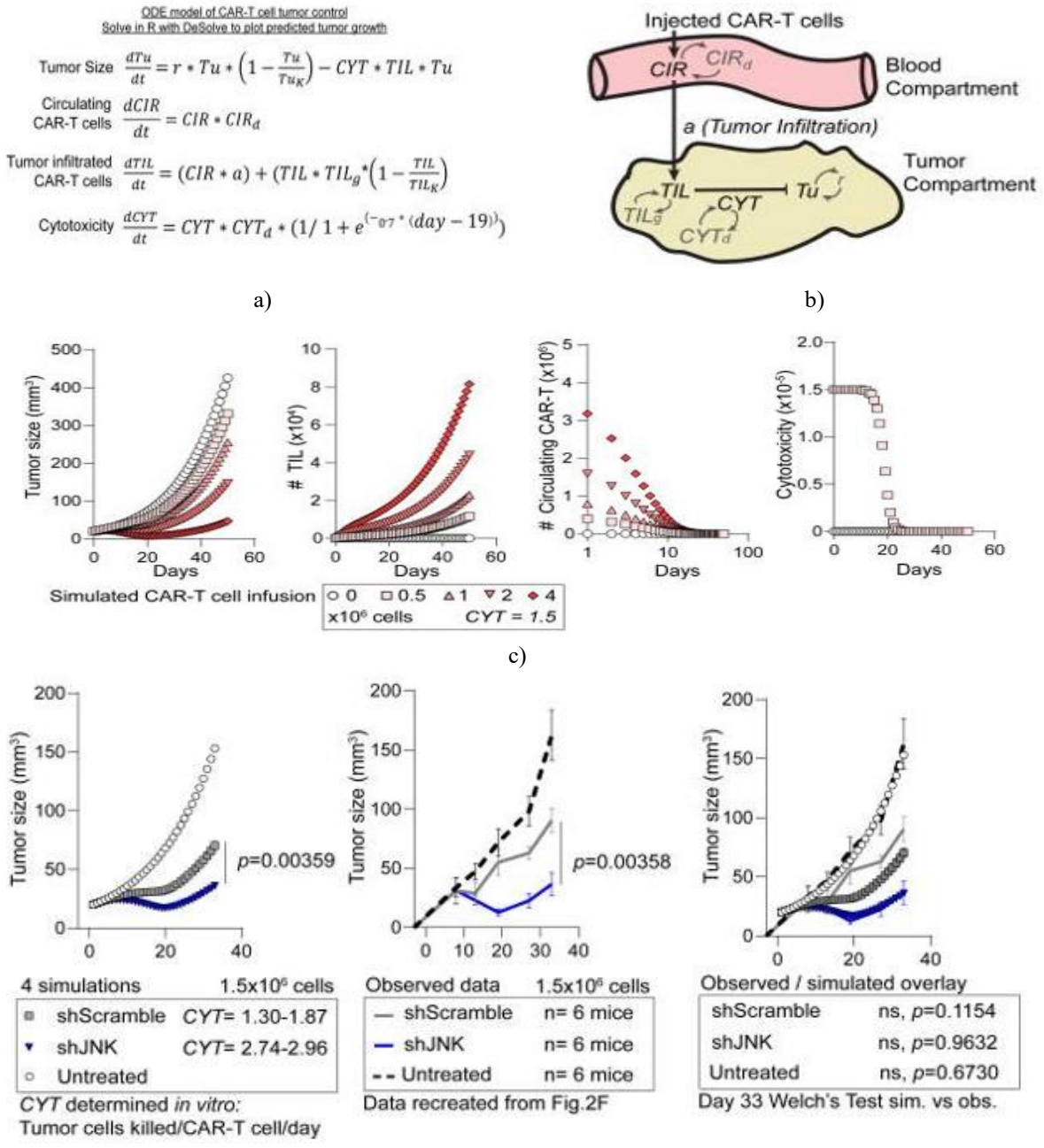

Figure 7. Mathematical modeling supports enhanced cytotoxicity as a mechanism for enhanced efficacy by JNK knockdown. (a) An ordinary differential equations (ODE) model of CAR-T cell therapy was constructed based on the Lotka-Volterra predator-prey framework. Each equation is labeled to describe its specific function, and DeSolve in R was used to solve the system and generate simulated tumor size trajectories. (b) Diagram illustrating the relationships between model parameters. (c) Model demonstration: tumor growth curves were simulated using CAR-T doses indicated after fitting the model to observed tumor progression in untreated and shJNK-treated mice. (d) In vitro cytotoxicity rates of shScramble and shJNK CAR-T cells were incorporated into four simulations of tumor growth, which were then overlaid with observed tumor growth curves from **Figure 2f**. Unpaired t-tests with Welch's correction were applied. a, tumor infiltration rate of circulating CAR-T cells; CAR-T, chimeric antigen receptor T; CIR, circulating CAR-T cell count; CYT, cytotoxicity; JNK, c-Jun N-terminal

kinases; ODE, ordinary differential equations; r, tumor growth rate; shScramble, scrambled short-hairpin RNA; TIL, tumor-infiltrated CAR-T cell count; Tu, tumor size; Xd, decay of "x"; Xg, growth of "x"; Xk, carrying capacity of "x".

We hypothesized that the superior tumor control observed with shJNK CAR-T cells was attributable to enhanced cytotoxicity. Using in vitro cytotoxicity measurements (shScramble: 1.30–1.87, shJNK: 2.77–2.96 tumor cells killed per CAR-T cell per day) while keeping other parameters constant, four simulations were performed. The higher cytotoxicity of shJNK CAR-T cells predicted significantly reduced tumor sizes by day 33, closely matching experimental tumor growth data **(Figure 7d)**. These results suggest that the observed in vitro cytotoxicity differences are sufficient to explain the enhanced antitumor efficacy in vivo.

Our findings demonstrate that JNK knockdown in CAR-T cells enhances cytotoxicity without affecting CAR-T cell production, differentiation, stemness, exhaustion, peripheral biodistribution, or tumor infiltration, highlighting its therapeutic potential. In vitro, JNK-depleted CD8+ CAR-T cells exhibited stronger cytotoxic activity driven by increased GZMB expression and degranulation **(Figure 4)**, consistent with prior evidence that GZMB overexpression enhances cytotoxicity [39]. Elevated GZMB persisted in CD8+ CAR-T cells ex vivo **(Figure 3)**, indicating maintained cytotoxic function within the tumor, although one experiment did not reach statistical significance, limiting data strength. The mathematical model **(Figure 7)** further confirmed that in vitro cytotoxicity differences could translate into substantial variations in tumor control in vivo. Overall, these data support a model in which enhanced tumor control is mediated via GZMB- and degranulation-dependent cytotoxicity.

Although JNK has been implicated in regulating NFATc1 [9], NFATc2 [11], and c-Jun pathways [40], our data indicate that GZMB upregulation following JNK knockdown primarily occurs through NFATc1. Both NFATc1 and NFATc2 bind the GZMB locus [6, 7], but only NFATc1 knockout blocked JNK-dependent GZMB induction **(Figure 5)**. NFATc1 overexpression alone was sufficient to restore high GZMB levels. Transcriptional profiling revealed strong enrichment of NFATc1-bound genes—but not c-Jun-bound genes—after JNK knockdown **(Figure 6)**. Mechanistically, we recapitulated prior findings showing enhanced NFATc1 nuclear localization following JNK suppression [9, 10]. Collectively, these results suggest that JNK knockdown promotes NFATc1 nuclear translocation, driving increased GZMB expression and cytotoxicity.

While our findings support an NFATc1-dependent mechanism, the interplay between NFATc1, NFATc2, and c-Jun remains incompletely resolved. For instance, NFATc2 knockout increased GZMB expression intensity, implying potential competitive interactions at the GZMB locus and possibly at other genomic sites that were not captured in our transcriptional assay. Additionally, reduced NFAT reporter activity **(Figure 1)** suggests potential alterations in NFAT/AP-1 interactions. Further investigation of these dynamics could inform optimization strategies for CAR-T cells.

Although direct manipulation of NFAT warrants further exploration, it is unclear whether this would provide greater therapeutic benefit than JNK knockdown. NFATc1 undergoes feed-forward amplification [10, 41], so overexpression could risk uncontrolled signaling and compromise CAR-T efficacy. In contrast, JNK knockdown enhanced cytotoxicity while preserving CAR-T differentiation, producing only modest reductions in overall cytokine production and activation marker expression. Thus, JNK knockdown appears to promote cytotoxicity via NFATc1 without triggering excessive activation, suggesting a favorable balance between efficacy and safety.

Our findings are consistent with prior studies linking JNK signaling, NFATc1 activity, and T cell cytotoxicity. Human T cells with impaired TCR-induced JNK signaling exhibited increased NFATc1 activity [10], and silencing MLK3, an upstream regulator of JNK, elevated GZMB expression through an NFATc1-dependent mechanism [42]. Similarly, deletion of JNK2 in OT-I T cells enhanced cytotoxicity and GZMB levels in murine breast cancer models [43]. In contrast, JNK1 deficiency reduced CD8+ T cell activation in murine breast cancer [44], and JNK inhibition has been associated with enhanced Th2 polarization [10, 45]. In our experiments, CAR-T cells with JNK knockdown showed no impairments in proliferation or differentiation **(Figure 1)**, likely because JNK was suppressed after initial CAR-T priming. Collectively, these results suggest that JNK predominantly restrains cytotoxic activity during the effector phase of CD8+ CAR-T cells without altering cell fate.

Most current strategies to enhance CAR-T efficacy focus on modifying differentiation, preventing exhaustion, or improving biodistribution [1, 4]. In contrast, direct approaches to augment cytotoxicity are scarce; for example, overexpression of granzymes increased killing but also accelerated CAR-T apoptosis and reduced in vivo persistence [39]. In our study, JNK knockdown augmented cytotoxicity without compromising CAR-T persistence, resulting in improved tumor control in vivo **(Figures 2 and 3)**. Nevertheless, shJNK CAR-T cells remained susceptible to exhaustion, suggesting that combining JNK suppression with interventions that prolong CAR-T longevity could produce synergistic effects for solid tumor therapy.

Beyond direct cytotoxicity, JNK knockdown may influence the tumor microenvironment by enhancing antigen release, thereby supporting the cancer immunity cycle [46]. However, these experiments were limited to xenograft models, and future studies should evaluate such effects in syngeneic murine and humanized models of ovarian cancer.

Conclusion

Our study demonstrates that JNK knockdown enhances CAR-T cell efficacy primarily by increasing cytotoxicity. This strategy is highly promising, as incorporation of the shJNK cassette into existing CAR constructs could substantially improve antitumor performance. Moreover, it is likely compatible with approaches that enhance CAR-T cell longevity and stem-like properties, potentially enabling sustained tumor eradication. Such enhancements could help overcome current limitations in CAR-T therapy for solid tumors.

Acknowledgments: Animal imaging was performed in the Small Animal Imaging Shared Facility at UAB supported by the O'Neal Comprehensive Cancer Center Grant P30CA013148. Flow cytometry was performed in the Flow Cytometry and Single Cell Core Facility at UAB supported by the Center for AIDS Research grant AI027767 and P30CA013148.

Conflict of Interest: None

Financial Support: This work was supported by the following grants: R01AI110200 (MK), R01CA232015 (MK), R01CA293907 (MK), 3P30CA013148-51S3 (MK), CRI5425 (MK), ChadTough Defeat DIPG Foundation grant (MK), Norma Livingston Ovarian Cancer Foundation grant (MK), and UAB ONCCC Pre-R01 (MK). Funding organizations were not directly involved in the study or its publication.

Ethics Statement: The University of Alabama at Birmingham Institutional Animal Care and Use Committee (IACUC) reviewed and approved the animal study under protocol 21938.

References

1. Agliardi G, Liuzzi AR, Hotblack A, et al. Intratumoral IL-12 delivery empowers CAR-T cell immunotherapy in a pre-clinical model of glioblastoma. Nat Commun. 2021;12:444. doi: 10.1038/s41467-020-20599-x.
2. Grosser R, Cherkassky L, Chintala N, et al. Combination Immunotherapy with CAR T Cells and Checkpoint Blockade for the Treatment of Solid Tumors. Cancer Cell. 2019;36:471–82. doi: 10.1016/j.ccell.2019.09.006.
3. Doan AE, Mueller KP, Chen AY, et al. FOXO1 is a master regulator of memory programming in CAR T cells. Nature. 2024;629:211–8. doi: 10.1038/s41586-024-07300-8.
4. Wei J, Long L, Zheng W, et al. Targeting REGNASE-1 programs long-lived effector T cells for cancer therapy. Nature. 2019;576:471–6. doi: 10.1038/s41586-019-1821-z.
5. Lee J-U, Kim L-K, Choi J-M. Revisiting the Concept of Targeting NFAT to Control T Cell Immunity and Autoimmune Diseases. Front Immunol. 2018;9:2747. doi: 10.3389/fimmu.2018.02747.
6. Klein-Hessling S, Muhammad K, Klein M, et al. NFATc1 controls the cytotoxicity of CD8+ T cells. Nat Commun. 2017;8:511. doi: 10.1038/s41467-017-00612-6.
7. Martinez GJ, Pereira RM, Äijö T, et al. The transcription factor NFAT promotes exhaustion of activated CD8+ T cells. Immunity. 2015;42:265–78. doi: 10.1016/j.immuni.2015.01.006.
8. Künkele A, Johnson AJ, Rolczynski LS, et al. Functional Tuning of CARs Reveals Signaling Threshold above Which CD8+ CTL Antitumor Potency Is Attenuated due to Cell Fas-FasL-Dependent AICD. Cancer Immunol Res. 2015;3:368–79. doi: 10.1158/2326-6066.CIR-14-0200.

9. Chow CW, Dong C, Flavell RA, et al. c-Jun NH(2)-terminal kinase inhibits targeting of the protein phosphatase calcineurin to NFATc1. Mol Cell Biol. 2000;20:5227–34. doi: 10.1128/MCB.20.14.5227-5234.2000.
10. Bauman BM, Stinson JR, Kallarakal MA, et al. Dominant interfering CARD11 variants disrupt JNK signaling to promote GATA3 expression in T cells. J Exp Med. 2025;222:e20240272. doi: 10.1084/jem.20240272.
11. Ortega-Pérez I, Cano E, Were F, et al. c-Jun N-terminal kinase (JNK) positively regulates NFATc2 transactivation through phosphorylation within the N-terminal regulatory domain. J Biol Chem. 2005;280:20867–78. doi: 10.1074/jbc.M501898200.
12. Rincón M, Flavell RA, Davis RA. The JNK and P38 MAP kinase signaling pathways in T cell-mediated immune responses. Free Radic Biol Med. 2000;28:1328–37. doi: 10.1016/s0891-5849(00)00219-7.
13. Damia G, Broggini M. Platinum Resistance in Ovarian Cancer: Role of DNA Repair. Cancers (Basel) 2019;11:119. doi: 10.3390/cancers11010119.
14. Chardin L, Leary A. Immunotherapy in Ovarian Cancer: Thinking Beyond PD-1/PD-L1. Front Oncol. 2021;11:795547. doi: 10.3389/fonc.2021.795547.
15. Cutri-French C, Nasioudis D, George E, et al. CAR-T Cell Therapy in Ovarian Cancer: Where Are We Now? Diagnostics (Basel) 2024;14:819. doi: 10.3390/diagnostics14080819.
16. Kranz E, Kuhlmann CJ, Chan J, et al. Efficient derivation of chimeric-antigen receptor-modified TSCM cells. Front Immunol. 2022;13:877682. doi: 10.3389/fimmu.2022.877682.
17. Iwano S, Sugiyama M, Hama H, et al. Single-cell bioluminescence imaging of deep tissue in freely moving animals. Science. 2018;359:935–9. doi: 10.1126/science.aaq1067.
18. Sanjana NE, Shalem O, Zhang F. Improved vectors and genome-wide libraries for CRISPR screening. Nat Methods. 2014;11:783–4. doi: 10.1038/nmeth.3047.
19. Wen J, Wu D, Qin M, et al. Sustained delivery and molecular targeting of a therapeutic monoclonal antibody to metastases in the central nervous system of mice. Nat Biomed Eng. 2019;3:706–16. doi: 10.1038/s41551-019-0434-z.
20. Estep BK, Kuhlmann CJ, Osuka S, et al. Skewed fate and hematopoiesis of CD34+ HSPCs in umbilical cord blood amid the COVID-19 pandemic. iScience. 2022;25:105544. doi: 10.1016/j.isci.2022.105544.
21. Lotka AJ. Analytical Note on Certain Rhythmic Relations in Organic Systems. Proc Natl Acad Sci USA. 1920;6:410–5. doi: 10.1073/pnas.6.7.410.
22. Barros LRC, Paixão EA, Valli AMP, et al. CARTmath-A Mathematical Model of CAR-T Immunotherapy in Preclinical Studies of Hematological Cancers. Cancers (Basel) 2021;13:2941. doi: 10.3390/cancers13122941.
23. Soetaert K, Petzoldt T, Setzer RW. Solving differential equations in R: package deSolve. J Stat Softw. 2010;33:1–25. doi: 10.18637/jss.v033.i09.
24. Klein-Hessling S, Muhammad K, Klein M, et al. NFATc1 controls the cytotoxicity of CD8+ T cells. Nat Commun . 2017;8:GSE98726. doi: 10.1038/s41467-017-00612-6.
25. Kurachi M, Barnitz RA, Yosef N, et al. The transcription factor BATF operates as an essential differentiation checkpoint in early effector CD8+ T cells. Nat Immunol . 2014;15:373–83. doi: 10.1038/ni.2834.
26. Bennett BL, Sasaki DT, Murray BW, et al. SP600125, an anthrapyrazolone inhibitor of Jun N-terminal kinase. Proc Natl Acad Sci U S A. 2001;98:13681–6. doi: 10.1073/pnas.251194298.
27. Wu Q, Wu W, Jacevic V, et al. Selective inhibitors for JNK signalling: a potential targeted therapy in cancer. J Enzyme Inhib Med Chem. 2020;35:574–83. doi: 10.1080/14756366.2020.1720013.
28. Davenport AJ, Cross RS, Watson KA, et al. Chimeric antigen receptor T cells form nonclassical and potent immune synapses driving rapid cytotoxicity. Proc Natl Acad Sci USA. 2018;115:E2068–76. doi: 10.1073/pnas.1716266115.
29. Trastuzumab: drug bank ID DB00072
30. Kranz E, Chan J, Hashimoto M, et al. Membrane-proximal external region is a superior target for mediating effector activity of hiv-1 specific chimeric antigen receptor modified t cells. bioRxiv. doi: 10.1101/2020.03.11.987610. Preprint.
31. Sun L, Su Y, Jiao A, et al. T cells in health and disease. Signal Transduct Target Ther. 2023;8:235. doi: 10.1038/s41392-023-01471-y.
32. Chovatiya N, Kaur K, Huerta-Yepez S, et al. Inability of ovarian cancers to upregulate their

MHC-class I surface expression marks their aggressiveness and increased susceptibility to NK cell-mediated cytotoxicity. Cancer Immunol Immunother. 2022;71:2929–41. doi: 10.1007/s00262-022-03192-7.

33. Brunell AE, Lahesmaa R, Autio A, et al. Exhausted T cells hijacking the cancer-immunity cycle: Assets and liabilities. Front Immunol. 2023;14:1151632. doi: 10.3389/fimmu.2023.1151632.
34. Ott E, Bilonda L, Dansette D, et al. The density of Tbet+ tumor-infiltrating T lymphocytes reflects an effective and druggable preexisting adaptive antitumor immune response in colorectal cancer, irrespective of the microsatellite status. Oncoimmunology. 2019;8:e1562834. doi: 10.1080/2162402X.2018.1562834.
35. Cassioli C, Baldari CT. The Expanding Arsenal of Cytotoxic T Cells. Front Immunol. 2022;13:883010. doi: 10.3389/fimmu.2022.883010.
36. Knörck A, Schäfer G, Alansary D, et al. Cytotoxic Efficiency of Human CD8+ T Cell Memory Subtypes. Front Immunol. 2022;13:838484. doi: 10.3389/fimmu.2022.838484.
37. Luo D, Luo H, Yan X, et al. Mycoplasma genitalium Protein of Adhesion Suppresses T Cell Activation via CypA-CaN-NFAT Pathway. Microbiol Spectr. 2023;11:e04503-22. doi: 10.1128/spectrum.04503-22.
38. Yin T, Wang G, Wang L, et al. Breaking NGF-TrkA immunosuppression in melanoma sensitizes immunotherapy for durable memory T cell protection. Nat Immunol. 2024;25:268–81. doi: 10.1038/s41590-023-01723-7.
39. Hay ZLZ, Kim DD, Cimons JM, et al. Granzyme F: Exhaustion Marker and Modulator of Chimeric Antigen Receptor T Cell-Mediated Cytotoxicity. J Immunol. 2024;212:1381–91. doi: 10.4049/jimmunol.2300334.
40. Dong C, Davis RJ, Flavell RA. Signaling by the JNK Group of MAP Kinases. J Clin Immunol. 2001;21:253–7. doi: 10.1023/A:1010975124110.
41. Chuvpilo S, Jankevics E, Tyrsin D, et al. Autoregulation of NFATc1/A expression facilitates effector T cells to escape from rapid apoptosis. Immunity. 2002;16:881–95. doi: 10.1016/s1074-7613(02)00329-1.
42. Kumar S, Singh SK, Viswakarma N, et al. Mixed lineage kinase 3 inhibition induces T cell activation and cytotoxicity. Proc Natl Acad Sci U S A. 2020;117:7961–70. doi: 10.1073/pnas.1921325117.
43. Tao J, Gao Y, Li MO, et al. JNK2 negatively regulates CD8+ T cell effector function and anti-tumor immune response. Eur J Immunol. 2007;37:818–29. doi: 10.1002/eji.200636726.
44. Gao Y, Tao J, Li MO, et al. JNK1 is essential for CD8+ T cell-mediated tumor immune surveillance. J Immunol . 2005;175:5783–9. doi: 10.4049/jimmunol.175.9.5783.
45. Conze D, Krahl T, Kennedy N, et al. c-Jun NH(2)-terminal kinase (JNK)1 and JNK2 have distinct roles in CD8(+) T cell activation. J Exp Med. 2002;195:811–23. doi: 10.1084/jem.20011508.
46. Mellman I, Chen DS, Powles T, et al. The cancer-immunity cycle: Indication, genotype, and immunotype. Immunity. 2023;56:2188–205. doi: 10.1016/j.immuni.2023.09.011.